Modelling of Air Release in Liquids

A. Klein*, U. Iben**

Robert Bosch GmbH, CR/ARH, P.O. Box 106050, 70049 Stuttgart, Germany

Abstract

Air release in hydraulic systems and components leads to a bubbly two-phase mixture with properties that are different from those of monophase liquids; e.g. altered in viscosity and speed of sound. As a result, the system eigenfrequencies change and noise may be generated. In most cases, the driving force of air release is a pressure drop induced shift in the solubility equilibrium. Different air release models are derived by means of conservation laws of mass, momentum and energy. The considerations are carried out for non-interacting bubbles in finite and infinite domains, where a spherical nucleus is the starting point of the analysis. In particular, the mass transfer of dissolved air is described by an advection-diffusion equation formulated in terms of Lagrangian coordinates. These are initialised on the phase boundary of spherical air bubbles. The solubility equilibrium is modelled in terms of Henry's law and the conservation of momentum leads to an extended Rayleigh-Plesset equation representing the bubble dynamics. In order to study and compare the properties of the models, the resulting differential equations are solved numerically. Thereby, the time-dependent diffusion boundary layer on the bubble surface is resolved by adapted grids. The simulations reveal that advection has to be considered for strong pressure gradients, which induce a velocity field around the air bubble. In contrast, slow bubble growth can be sufficiently described by the diffusion equation in the case of small bubbles. Thermal effects play a minor role for pressure oscillations outside the eigenfrequency of the air bubble and common liquids such as water or oils.

Keywords: air release, gaseous cavitation, two phase flow, diffusion-induced bubble growth, numerical simulation

1. Introduction

Fluids such as water and oils used in technical applications may contain a limited amount of dissolved air. The thermodynamic state of a solute-solvent-system is determined by the solubility equilibrium, which depends on temperature T and pressure p. Therefore, the process of heterogeneous nucleation and subsequent growth of the gaseous phase, denoted as air release, sets in when system pressure or temperature changes. Air release plays an important role in hydraulic systems and components, e.g. breaking systems of cars or piston pumps controlled by suction valves. Air release leads to a bubbly two-phase mixture that has different properties than the monophase liquid. Consequently, the density, the speed of sound as well as the viscosity of the two-phase mixture change rapidly in time and space. Local properties of air-liquid mixtures strongly influence a system's hydraulic functionalities, such as it's volume flow rate and pressure drops. As a result, the system eigenfrequencies change and noise may be generated.

Numerical simulations have typically been used to design and characterise hydraulic systems or components. For these simulations, robust and numerically efficient methods and models have to be available. Identifying air release models suitable for computational fluid dynamics or one-dimensional system simulations is a key task for the near future. In this paper air release models are presented and discussed. Non-interacting, spherical bubbles in finite and infinite liquid domains form the basis for our analysis. Different models are derived by conservation laws of mass, momentum and energy. In addition, the mechanical equilibrium and mechanical non-equilibrium are considered. The resulting differential equations are solved numerically in order to study and compare the properties of these models.

2. Formulation of the Problem

In this paper a spherical nuclei is the starting point to model air release in liquid-gas solutions. We assume that at the initial time $t = 0$ a spherical bubble of radius R_0 is placed in a finite liquid-gas solution in which the initial molare concentration of dissolved gas is uniform and equal to $c_{\mathrm{L},0}$. The centre of the bubble is taken as origin of a spherical polar coordinate system as shown in Fig. 1(a). That way, the derived models may be applied in the context of a homogeneous two-phase mixture; where a bubble is transported in a liquid without relative motion.

The bubble growth as shown in Fig. 1(b) states a three-dimensional, time-dependent problem. In order to model air release in a mathematically simplified way the problem is reduced in complexity using the following assumptions:

*Corresponding author, alexander.klein4@de.bosch.com
**Presenting author, uwe.iben@de.bosch.com

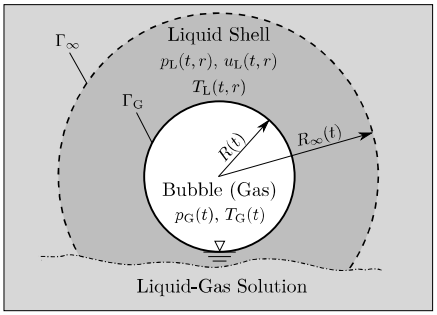

(a) Spherical model

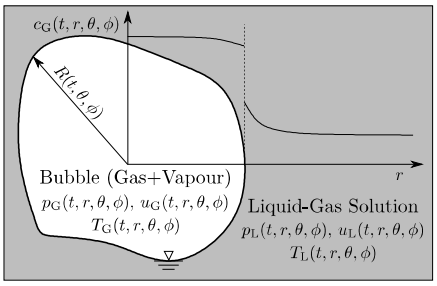

(b) Real situation

Fig. 1: Schematic diagram of a bubble in a liquid-gas solution. The modelled control volume of the solution, denoted as liquid shell in Fig. 1(a), is bounded such that $R(t) \leq r \leq R_\infty(t)$ and exhibits the time-dependent boundaries Γ_∞ and Γ_G. Fig. 1(b) shows the real situation of a non-spherical bubble in an arbitrary three-dimensional temperature, pressure and velocity field. The concentration profile in one spatial direction of a dissolving bubble is shown as an example.

1. The gaseous phase is composed of air, contains no solvent vapour and is described by the ideal gas law of a pure substance. Furthermore, any pressure and temperature gradients within the bubble are disregarded as discussed by Plesset and Zwick for vapour bubbles in superheated liquids [16]. The solubility of air in the solvent is assumed to be low such that the mole fraction is less than 1 %.
2. The physical properties of the involved fluids are supposed to be constant over moderate variations of temperature and pressure. In particular, the properties of the gas-liquid solution are independent of the solute's mole fraction and adequately modelled by an ideal dilute solution. The solvent is described as pure Newtonian fluid leading to a binary system in which chemical reactions are absent.
3. The former assumptions allow us to express the solubility equilibrium on the phase boundary in terms of Henry's law (see Ref. [12]), which reads
$$c_L|_{r=R} = c_G = p_G\, H(T_L|_{r=R}) \;, \tag{1}$$
where c_G is the molar concentration in the solution on the sharp phase boundary and p_G is the pressure in the gas phase. The Henry coefficient H can be expressed as a function of temperature for moderate pressure conditions, cf. Lucas [12]. According to eq. 1 the bubble surface is supposed to return to the solubility equilibrium instantaneously when either the bubble temperature $T_G = T_L|_{r=R}$ or the pressure p_G changes.
4. Compressibility effects in the liquid phase are neglected since the velocity of the bubble surface $\dot{R}$ is supposed to be much smaller than the speed of sound, $\dot{R} \ll a_L$.
5. Fourier's and Fick's law are applied to model diffusive heat and mass transfer with a constant isotropic thermal diffusivity β_T and diffusion coefficient β_D, respectively.
6. The kinetic energy of the system and viscous dissipation are disregarded in the energy balance. Additionally, the change in enthalpy of the solvent with pressure is neglected over moderate variations of system pressure.
7. The Rayleigh-Plesset equation is extended for a finite system as shown by Arefmanesh et al. and used to describe bubble dynamics [1]. This implies the mass flow across the phase boundary is neglected in the momentum balance on the bubble surface, cf. Brennen [4].

2.1. Conservation of Mass

The mass balance for the bubble can be expressed in terms of the mass flow rate $\dot{m}_G$ of gas into the bubble

$$\dot{m}_G = 4\pi R^2 \beta_D M_G \left.\frac{\partial c_L}{\partial r}\right|_{r=R} \;, \tag{2}$$

where β_D is the diffusion coefficient of the solute in the solvent and M_G the molare mass of the solute. A correction term accounting for the selectively-permeable properties of the bubble surface is left out of the model due to the low solubility of the solute (recall that in agreement with assumption 1 no solvent vapour permeates the surface). Considering a spherical problem, the equation of continuity yields for the radial velocity in the liquid phase, cf. Brennen [4],

$$u_L(t,r) = \left(\frac{R}{r}\right)^2 \dot{R} \;. \tag{3}$$

The mass flow rate $\dot{m}_G$ depends on the gradient of the concentration field on the bubble surface $\left.\frac{\partial c_L}{\partial r}\right|_{r=R}$ that is determined by the advection-diffusion equation. Taking into account eq. 3 the transport equation reads

$$\frac{\partial c_L}{\partial t} + u_L \frac{\partial c_L}{\partial r} = \frac{\beta_D}{r^2}\frac{\partial}{\partial r}\left(r^2 \frac{\partial c_L}{\partial r}\right) \;, \quad R(t) \leq r \leq R_\infty(t) \;. \tag{4}$$

The partial differential equation (PDE) is subject to initial and boundary conditions. At the initial time $t = 0$ there is a uniform concentration field of solute in the solution

except for the specific concentration on the bubble surface given by the solubility equilibrium,

$$t = 0: \; c_{\mathrm{L}}|_{t=0, r>R} = c_{\mathrm{L},0} \; , \tag{5}$$

$$\Gamma_{\mathrm{G}}: \; c_{\mathrm{L}}|_{t\geq 0, r=R} = c_{\mathrm{G}} = p_{\mathrm{G}}\, H(T_{\mathrm{G}}) \; , \tag{6}$$

$$\Gamma_{\infty}: \; \left.\frac{\partial c_{\mathrm{L}}}{\partial r}\right|_{t\geq 0, r=R_{\infty}} = 0 \; . \tag{7}$$

A further constraint of the system is a constant mass of solvent in the liquid shell yielding

$$R_{\infty}^3 - R^3 = \left(R_{\infty}^3 - R^3\right)\big|_{t=0} \; . \tag{8}$$

The latter two equations result in a finite pool of solute in the system, since no mass transport is allowed to occur across the outer boundary Γ_{∞}.

The presented boundary conditions are a model for an activated nuclei that starts to grow in a finite system at the time $t = 0$. The problem stated by eq. 2 to 8 is a moving boundary problem, more precisely a Stefan problem, cf. Winzer [21]. The closure condition that expresses the motion of the phase boundary as a function of quantities determined by the solution of the underlying PDE is given by eq. 2 considering that the mass flow rate $\dot{m}_{\mathrm{G}}$ determines the local velocity of the phase boundary. Applying Lagrangian coordinates to the Stefan Problem

$$\tilde{t} \overset{\mathrm{def}}{=} t \quad \text{and} \quad \tilde{r} \overset{\mathrm{def}}{=} r^3 - R^3 \; , \tag{9}$$

we ease the mathematical treatment of the moving boundary problem analogous to previous works [1, 3, 15]. Combining eq. 4, 8 and 9, the transformed advection-diffusion equation exhibits time-independent boundaries and reads

$$\begin{aligned} \frac{\partial c_{\mathrm{L}}}{\partial t} &= 9\beta_{\mathrm{D}} \frac{\partial}{\partial \tilde{r}} \left(\left(\tilde{r} + R^3\right)^{\frac{4}{3}} \frac{\partial c_{\mathrm{L}}}{\partial \tilde{r}} \right) \; , \\ 0 \leq \tilde{r} &\leq \left(R_{\infty} - R^3\right)\big|_{t=0} \; . \end{aligned} \tag{10}$$

A general analytical solution to eq. 4 or 10 is unknown to the present authors. Neglecting the convective term in eq. 4 results in the diffusion equation

$$\frac{\partial c_{\mathrm{L}}}{\partial t} = \frac{\beta_{\mathrm{D}}}{r^2} \frac{\partial}{\partial r} \left(r^2 \frac{\partial c_{\mathrm{L}}}{\partial r} \right) \; , \tag{11}$$

the solution of which is given by Carslaw [6] for a infinite system, $R_{\infty} \to \infty$, and applied to the problem of bubble growth by Epstein and Plesset [8]. The initial and boundary condition on the inner surface are given by eq. 5 and 6, respectively. The boundary condition on the outer surface is, contrary to the boundary condition of the advection-diffusion (eq. 4), given by

$$\Gamma_{\infty}: \; c|_{t, r\to\infty} = c_{\mathrm{L},0} \; , \tag{12}$$

and violates the claim in this paper to model a finite system. Therefore, the concentration gradient on the bubble surface, which is given by the analytical solution of the diffusion equation, is extend to fullfill the total mass balance of a finite system. This yields an approximated gradient of the solute concentration on the bubble surface

$$\left.\frac{\partial c_{\mathrm{L}}}{\partial r}\right|_{r=R} = \frac{c_{\mathrm{L},0} - \frac{m_{\mathrm{G}} - m_{\mathrm{G},0}}{M_{\mathrm{G}} V_{\mathrm{L}}} - c_{\mathrm{G}}}{R} \left(1 + \frac{R}{\sqrt{\pi \beta_{\mathrm{D}} t}}\right) \; . \tag{13}$$

In the limiting case of an infinite system eq. 13 approaches the original gradient determined by Epstein and Plesset. Disregarding the time-dependent term in the approximated gradient yields a constant Sherwood number $\mathrm{Sh} = 2$ (for a definition of the Sherwood number cf. Baehr [2]).

2.2. Conservation of Momentum

The motion of the incompressible Newtonian liquid surrounding the bubble is governed by the conservation law of momentum, which reads for a spherical problem

$$\begin{aligned} \rho_{\mathrm{L}} \left(\frac{\partial u_{\mathrm{L}}}{\partial t} + u_{\mathrm{L}} \frac{\partial u_{\mathrm{L}}}{\partial r} \right) = \\ - \frac{\partial p_{\mathrm{L}}}{\partial r} + \rho_{\mathrm{L}} \nu_{\mathrm{L}} \left[\frac{1}{r^2} \frac{\partial}{\partial r} \left(r^2 \frac{\partial u_{\mathrm{L}}}{\partial r} \right) - \frac{2}{r^2} u_{\mathrm{L}} \right] \; , \end{aligned} \tag{14}$$

where the kinematic viscosity ν_{L} is approximated by the solvent subject to assumption 2. Substituting the velocity field from eq. 3 and integrating in radial direction from Γ_{G} to Γ_{∞}, we obtain

$$\begin{aligned} p_{\mathrm{L}}|_{r=R} - p_{\mathrm{L}}|_{r=R_{\infty}} = \\ \rho_{\mathrm{L}} \left[\frac{\dot{R}^2}{2} \left(\frac{R^4}{R_{\infty}^4} - 1 \right) - \left(R\ddot{R} + 2\dot{R}^2 \right) \left(\frac{R}{R_{\infty}} - 1 \right) \right] \; . \end{aligned} \tag{15}$$

In accordance with assumption 7 the balance of forces is used to compute the pressure drop over the inner and outer boundary of the control volume shown in Fig. 2(a),

$$p_{\mathrm{G}} - p_{\mathrm{L}}|_{r=R} = 4\rho_{\mathrm{L}}\nu_{\mathrm{L}} \frac{\dot{R}}{R} + \frac{2\sigma_{\mathrm{L}}}{R} \; , \tag{16}$$

$$p_{\infty} - p_{\mathrm{L}}|_{r=R_{\infty}} = 4\rho_{\mathrm{L}}\nu_{\mathrm{L}} \frac{R^2 \dot{R}}{R_{\infty}^3} \; . \tag{17}$$

The pressure inside the bubble p_{G} differs from the pressure on the outside $p_{\mathrm{L}}|_{r=R}$ due to the surface tension σ_{L} and the local velocity of the surface $\dot{R}$. Combining eq. 15, 16 and 17 gives an extended Rayleigh-Plesset equation describing the bubble dynamics

$$\begin{aligned} (p_{\mathrm{G}} - p_{\infty}) = \frac{2\sigma_{\mathrm{L}}}{R} - \frac{4\rho_{\mathrm{L}}\nu_{\mathrm{L}}\dot{R}}{R} \left(\frac{R^3}{R_{\infty}^3} - 1 \right) + \\ \rho_{\mathrm{L}} \left[\frac{\dot{R}^2}{2} \left(\frac{R^4}{R_{\infty}^4} - 1 \right) - \left(R\ddot{R} + 2\dot{R}^2 \right) \left(\frac{R}{R_{\infty}} - 1 \right) \right] \; . \end{aligned} \tag{18}$$

The latter equation can be linearised for the limiting case of an infinite system, $R_{\infty} \to \infty$, yielding the representation of a damped oscillator with the undamped angular frequency

$$\omega_0 = \sqrt{\frac{3\kappa p_{\infty,0}}{\rho_{\mathrm{L}} R_0^2} + \frac{2\sigma_{\mathrm{L}}}{\rho_{\mathrm{L}} R_0^3} (3\kappa - 1)} \; , \tag{19}$$

where $\kappa = 1$ denotes an isothermal and $\kappa = 1.4$ an isentropic and adiabatic bubble, cf. Ref. [14]. In the limiting case of slow bubble growth, $\dot{R} \to 0$, eq. 18 simplifies to the mechanical equilibrium of a bubble in a static fluid

$$p_\mathrm{G} = p_\mathrm{L} + \frac{2\sigma_\mathrm{L}}{R} \ . \tag{20}$$

2.3. Conservation of Energy

The conservation of energy for the air bubble requires the change of internal energy $\frac{dU_\mathrm{G}}{dt}$ to be equal to the sum of heat transfer $\dot{Q}_\mathrm{G}$, energy change due to a change in the bubble volume V_G and energy transfer due to mass transport across the control surface, cf. Fig. 2(b),

$$\frac{dU_\mathrm{G}}{dt} = \dot{Q}_\mathrm{G} + \dot{W}_\mathrm{G} + \dot{m}_\mathrm{G} h_\mathrm{G,L} \ , \text{ where} \tag{21}$$

$$U_\mathrm{G} = m_\mathrm{G} h_\mathrm{G} - p_\mathrm{G} V_\mathrm{G} \ , \tag{22}$$

$$\dot{Q}_\mathrm{G} = 4\pi R^2 \lambda_\mathrm{L} \left.\frac{\partial T_\mathrm{L}}{\partial r}\right|_{r=R} \ , \tag{23}$$

$$\dot{W}_\mathrm{G} = -p_\mathrm{G} \dot{V}_\mathrm{G} \text{ and } V_\mathrm{G} = \frac{4}{3}\pi R^3 \ . \tag{24}$$

The dissolution of a gas in a solvent can be associated with a change in enthalpy, which is given by the enthalpy of solution Δh_L. Finally, the energy balance of the bubble reads

$$\dot{m}_\mathrm{G}\left[\Delta h_\mathrm{L} - \frac{\tilde{R} T_\mathrm{G}}{M_\mathrm{G}}\right] + m_\mathrm{G}\dot{T}_\mathrm{G}\left(c_\mathrm{p,G} - \frac{\tilde{R}}{M_\mathrm{G}}\right) = 4\pi R^2 \lambda_\mathrm{L} \left.\frac{\partial T_\mathrm{L}}{\partial r}\right|_{r=R} + 4\pi p_\mathrm{G} R^2 \dot{R} \ . \tag{25}$$

The energy balance of the liquid shell is expressed in terms of a transport equation. Assumption 6 allows us to model the heat transport in the liquid phase analogously to the mass transport, cf. eq. 10,

$$\frac{\partial T_\mathrm{L}}{\partial t} = 9\beta_\mathrm{T} \frac{\partial}{\partial \tilde{r}}\left(\left(\tilde{r} + R^3\right)^{\frac{4}{3}} \frac{\partial T_\mathrm{L}}{\partial \tilde{r}}\right) \ , \tag{26}$$

$$t = 0: \quad T_\mathrm{L}|_{t=0,\tilde{r}} = T_\mathrm{L,0} \ , \tag{27}$$

$$\Gamma_\mathrm{G}: \quad T_\mathrm{L}|_{t,\tilde{r}=0} = T_\mathrm{G} \ , \tag{28}$$

$$\Gamma_\infty: \quad \left.\frac{\partial T_\mathrm{L}}{\partial \tilde{r}}\right|_{t,\tilde{r}=(R_\infty - R^3)|_{t=0}} = 0 \ , \tag{29}$$

where Lagrangian coordinates are applied as well. The approximated gradient of a transport quantity on the bubble surface according to eq. 13 can also be used to express the temperature gradient on the bubble surface. At the initial time the system is at its thermal equilibrium. Furthermore, the characteristic time scale of heat transport $\tau_\mathrm{T} = \frac{R_0^2}{\beta_\mathrm{T}}$ is smaller than the characteristic time scale of mass transport $\tau_\mathrm{D} = \frac{R_0^2}{\beta_\mathrm{D}}$ such that $\tau_\mathrm{I} \ll \tau_\mathrm{T} < \tau_\mathrm{D}$, where $\tau_\mathrm{I} = \frac{\rho_\mathrm{L}\nu_\mathrm{L}}{p_{\infty,0}}$ is the characteristic time scale of bubble dynamics. Therefore, the system is likely to show only small temperature changes and the temperature gradient on the bubble surface is approximated by the stationary solution of the transport equation

$$\left.\frac{\partial T_\mathrm{L}}{\partial r}\right|_{r=R} = \frac{\bar{T}_\mathrm{L} - T_\mathrm{G}}{R} \ , \text{ where} \tag{30}$$

$$\bar{T}_\mathrm{L} = \frac{V_\mathrm{L}\rho_\mathrm{L} c_\mathrm{p,L} T_\mathrm{L,0} + (m_\mathrm{G,0} - m_\mathrm{G})(c_\mathrm{p,G} T_\mathrm{G} + \Delta h_\mathrm{L})}{\rho_\mathrm{L} V_\mathrm{L} c_\mathrm{p,L} + [(m_\mathrm{G,0} - m_\mathrm{G}) + c_\mathrm{L,0} V_\mathrm{L} M_\mathrm{G}]\, c_\mathrm{p,G}} - \frac{m_\mathrm{G,0}(T_\mathrm{G} - T_\mathrm{G,0}) + c_\mathrm{L,0} V_\mathrm{L} M_\mathrm{G} c_\mathrm{p,G} T_\mathrm{L,0}}{\rho_\mathrm{L} V_\mathrm{L} c_\mathrm{p,L} + [(m_\mathrm{G,0} - m_\mathrm{G}) + c_\mathrm{L,0} V_\mathrm{L} M_\mathrm{G}]\, c_\mathrm{p,G}} \ . \tag{31}$$

This means a constant Nusselt number $\mathrm{Nu} = 2$ for the heat transfer on the bubble surface, cf. Refs. [2, 10].

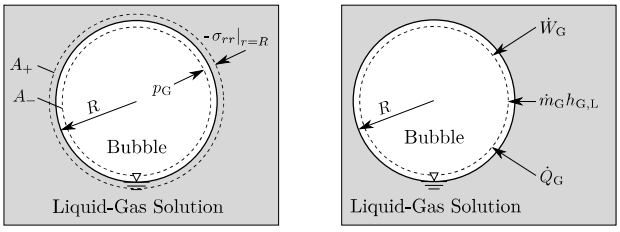

(a) Balance of forces **(b)** Energy balance

Fig. 2: Balance of forces and energy on the bubble surface. The control volume in Fig. 2(a) envelopes the sharp phase boundary of the bubble ($A_+ = A_-$). The radial stress on the phase boundary is denoted by $\sigma_{rr}|_{r=R} = -\,p_\mathrm{L}|_{r=R} + 2\rho_\mathrm{L}\nu_\mathrm{L}\frac{\partial u_\mathrm{L}}{\partial r}$, cf. Brennen [4].

3. Numerical Implementation

Different air release models, which vary in the quality of physical modelling, are deduced from the presented equations. Eq. 2 describes the mass growth of the bubble and is part of all models, whereas the remaining equations are as follows:

EI Energy and mass transport are modeled with transport eq. 10 and 26, respectively. The bubble dynamics are covered by eq. 18 and the energy balance of the bubble is given by eq. 25.

EI-EP-Nu2 The model is derived from the previous one by replacing the transport equation of mass with the approximated gradient by Epstein and Plesset, eq. 13, and the temperature gradient with eq. 30 ($\mathrm{Nu} = 2$). This yields a computationally efficient algorithm to model air release.

I The energy balance is disregarded and replaced by the assumption of an isothermal system. The mass transport is modeled with transport eq. 10. As with model EI and EI-EP-Nu2 the bubble dynamics are covered by eq. 18.

M Model I is further simplified by replacing the extended Rayleigh-Plesset equation with the mechanical equilibrium at the bubble surface, eq. 20. The mass transport in the liquid phase is still modeled with the PDE.

M-EP A simplification of model M where the transport equation is replaced with the approximated gradient by Epstein and Plesset, eq. 13.

M-Sh2 This is the most simple model presented in this paper. It is a simplification of model M where the transport equation is replaced with the approximated gradient by Epstein and Plesset disregarding the time-dependent term in eq. 13 (Sh = 2).

In order to improve numerical handling, the various sets of equations are transformed to a dimensionless representation given by

$$t^* = \frac{t}{\tau} \,, \qquad \tilde{r}^* = \frac{\tilde{r}}{(R_\infty^3 - R^3)|_{t=0}} \,, \tag{32}$$

$$R^* = \frac{R}{R_0} \,, \qquad p^* = \frac{p}{\bar{p}_\infty} \,, \tag{33}$$

$$c^* = \frac{c}{c_{\mathrm{L},0}} \,, \qquad T^* = \frac{T}{T_{\mathrm{L},0}} \,, \tag{34}$$

$$m_{\mathrm{G}}^* = \frac{m_{\mathrm{G}}}{m_{\mathrm{G},0}} \,. \tag{35}$$

As spatial discretisation a finite difference scheme according to Skeel and Berzins [18] is applied to the transport equations of mass and heat transfer resulting in a system of coupled ordinary differential equations (ODE). An implementation of backward differentiation formulas (BDF, cf. Ref. [17]) is used as timestepping method, since the underlying ODE system revealed itself to be stiff. The concentration and temperature boundary layer on the bubble surface are time-dependent and change their spatial dimension due to diffusive and advective transport. Therefore, each boundary layer thickness is computed at every numerical time step and the grid is adapted as needed. A logarithmic grid spacing ensures an adequate resolution near the phase boundary.

4. Results and Discussion

Air release is simulated for systems consisting of air and water for which fluid data are taken from various sources, cf. Refs. [5, 9, 11, 19, 20]. The models are solved numerically as described in the previous section, where arbitrary pressure curves as function of time can be given as input. The initial degree of saturation s_0 denotes the condition of the solution with regard to the solubility equilibrium at the beginning of a simulation

$$s_0 = \frac{c_{\mathrm{L},0}}{p_{\infty,0} H(T_{\mathrm{L},0})} \begin{cases} > 1 & \text{, oversaturated} \\ = 1 & \text{, saturated} \\ < 1 & \text{, undersaturated.} \end{cases} \tag{36}$$

Fig. 3 shows the response of a bubble excited by a single pressure oscillation. At a frequency near the bubble eigenfrequency model EI* and I* clearly show a post-pulse oscillation, cf. Fig. 3(a). Model EI* produces a higher eigenfrequency than model I*, which is in accordance with eq. 18. As can be seen in Fig. 3(b) the bubble dynamics may be neglected for moderate pressure oscillations, i.e. those with $f \leq 0.1\, f_{\mathrm{D}}$. The mechanical equilibrium on the bubble surface (model M) may be applied as adequate approximation in such cases. Moreover, simulations with model I and EI disclose bubbles to be excited by mass transfer under constant ambient pressure conditions (without Fig.), though this effect plays only a minor role in technical applications due to the small amplitudes encountered in such simulations.

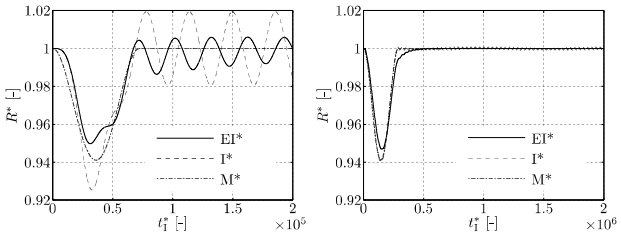

(a) $f = 0.5\, f_{\mathrm{D}}$ **(b)** $f = 0.125\, f_{\mathrm{D}}$

Fig. 3: Bubble dynamics at different excitation frequencies f of the ambient pressure

$$p_\infty = \begin{cases} \bar{p}_\infty - \hat{p}_\infty \left(\frac{\cos(2\pi f t) - 1}{2} \right) & , \; 0 \leq t \leq \frac{1}{f} \\ \bar{p}_\infty & , \; \frac{1}{f} \leq t \,. \end{cases}$$

with $\hat{p}_\infty = 0.2$ bar and $\bar{p}_\infty = 1$ bar. The initial bubble radius is $R_0 = 10^{-3}$ m and the bubble eigenfrequency is $f_{\mathrm{D}} = 2760$ Hz. Due to the short period of time in comparison with the timescale of heat and mass transfer, the transport equations are disabled in this simulations (denoted by an asterisk) yielding numerical efficient models to describe bubble dynamics. As a consequence, model EI* represents an adiabatic and isentropic bubble.

The models of air release presented in this paper are dependent on ten fluid properties denoted as z_i: β_{D}, $c_{\mathrm{p,G}}$, $c_{\mathrm{p,L}}$, H, Δh_{L}, λ_{L}, M_{G}, ν_{L}, ρ_{L} and σ_{L}. We use a sensitivity analysis to compute the variation of the dimensionless bubble mass with the relative change of a single fluid property z_i

$$z_i \frac{dm_{\mathrm{G}}^*}{dz_i} \approx z_i \frac{m_{\mathrm{G},i}^* - m_{\mathrm{G}}^*}{\Delta z_i} \,, \; i = 1, \ldots, 10 \,, \tag{37}$$

where $m_{\mathrm{G},i}^*$ is the bubble mass of the simulation performed with the disturbed set of fluid properties. The initial conditions, such as the amount of dissolved air, are unaltered in the sensitivity analysis. Fig. 4 shows the most influencing fluid properties of model EI-EP-Nu2, from which the Henry coefficient H and the diffusion coefficient β_{D} are the most dominant ones. This verifies air release to be a process activated by a change in the solubility equilibrium but inhibited by diffusive mass transport. The surface tension σ_{L} plays a major role for small bubbles in the order of several µm, cf. Fig. 4(b). The sensitivity analysis further indicates that energy related quantities, e.g. heat capacity c_{p} and thermal conductivity λ_{L}, are of mi-

nor importance for air release. This fact is also confirmed by simulations comparing model EI and I (without Fig.).

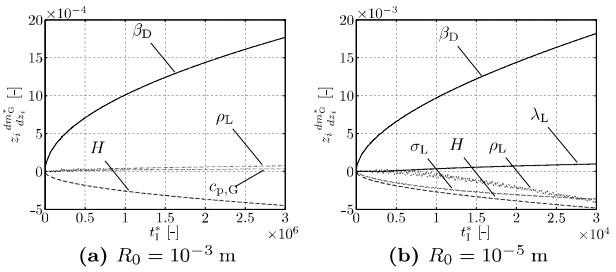

(a) $R_0 = 10^{-3}$ m **(b)** $R_0 = 10^{-5}$ m

Fig. 4: Sensitivity analysis of bubbles excited near their eigenfrequency. The ambient pressure is given by $p_\infty = \bar{p}_\infty + \hat{p}_\infty \sin(2\pi f t)$, with $\bar{p}_\infty = 1$ bar, $\hat{p}_\infty = 0.2$ bar and $f = 0.5\, f_D$. The initial degree of saturation is $s_0 = 5$ and the used model is EI-EP-Nu2.

Rectified diffusion denotes the process of bubble growth in undersaturated solutions due to pressure oscillations, cf. Refs. [7, 13]. It mainly consists of three effects:

1. The solubility equilibrium depends on the pressure in the gas phase (cf. eq. 1) and, therefore, an oversaturated solution may exist for a short fraction of time.
2. The surface area of an expanded bubble is much greater than that of a compressed bubble. Hence, the mass flow of air passing the bubble surface during its expansion is greater than the mass flow during its compression. Due to effect 1 an oversaturated solution may exist in times of an expanded bubble leading to a net mass flow of air into the gas phase.
3. The concentration gradient of dissolved air at the bubble surface is related to the boundary layer thickness. When the bubble expands, the boundary layer becomes thinner and the concentration gradient as well as the mass flow rate increases, cf. eq. 2. This effect is a result of the velocity field and the spherical symmetry of the problem.

As a result, rectified diffusion can counteract the dissolution process in an undersaturated solution for values of the pressure amplitude greater than a specific value

$$\left.\frac{\hat{p}_\infty}{\bar{p}_\infty}\right|_{RD} = \binom{3}{2}^{\frac{1}{2}} \left[1 + \frac{2\sigma_L}{R_0 \bar{p}_\infty} - s_0\right]^{\frac{1}{2}} , \qquad (38)$$

which is valid for oscillations much smaller than the bubble's eigenfrequency, cf. Eller and Flynn [7].

Fig. 5 shows the results of a simulation with $\frac{\hat{p}_\infty}{\bar{p}_\infty} > \left.\frac{\hat{p}_\infty}{\bar{p}_\infty}\right|_{RD} = 0.5$, so that the bubble mass is supposed to increase. Both models reflect effect 1 and 2, but only model M, which incorporates advective mass transport (effect 3), is able to reproduce rectified diffusion, cf. Fig. 5(a). As expected, this model also shows a decrease in bubble mass for $\frac{\hat{p}_\infty}{\bar{p}_\infty} < \left.\frac{\hat{p}_\infty}{\bar{p}_\infty}\right|_{RD}$ (without Fig.). Effect 3 is illustrated in Fig. 5(b), where the change of the dimensionless boundary layer thickness δ_D^* with ambient pressure can be seen. Such a behaviour can not be reproduced with model M-EP, since the advective mass transport is neglected. This is further illustrated by the comparison of the concentration profiles of dissolved air in the liquid phase, cf. Figs. 5(c) and 5(d). Model M produces complex concentration profiles that exhibit local maxima resulting in a net mass flow of air into the bubble even though the solution is undersaturated

$$\left.\frac{\partial c_L}{\partial r}\right|_{r=R} > 0 \text{ , for } c_G > c_L(r \to R_\infty) \text{ .} \qquad (39)$$

In contrast, model M-EP fails to produce such a behaviour. This result demonstrates the importance of advective mass transport during pressure oscillations in undersaturated solutions.

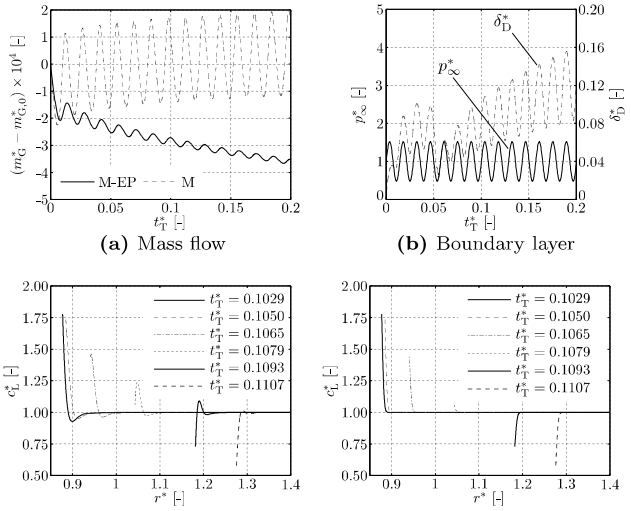

(a) Mass flow **(b)** Boundary layer

(c) Concentration profile considering advection and diffusion **(d)** Concentration profile considering diffusion

Fig. 5: Bubble Growth in an undersaturated solution during moderate pressure oscillations. The ambient pressure is given by $p_\infty = \bar{p}_\infty + \hat{p}_\infty \sin(2\pi f t)$, with $\bar{p}_\infty = 6$ bar, $\hat{p}_\infty = 0.52$ bar and $f = 10$ Hz. The initial degree of saturation and bubble size are $s_0 = \frac{5}{6}$ and $R_0 = 10^{-3}$ m, respectively.

Advective mass transport is also important for bubble growth in oversaturated solutions. As can be seen in Figs. 6(a) and 6(b) the difference in model M and M-EP increases with pressure amplitude. Model M predicts an increase in the bubble mass of 52 %, whereas model M-EP estimates an increase of 24 %. These relations are also valid for simulations of much smaller bubbles, cf. Fig. 6(c) and 6(d).

Model M-Sh2 can be reduced to a single ODE resulting in a simple but robust air release model. The more advanced models depend on the history of bubble growth. Model M-EP incorporates a time-dependent term in eq. 13 and models that solve a PDE also depend on the history of bubble growth. That is why model M-Sh2 compares badly with M and M-EP in Fig. 6(a) and 6(b). The stationary solution of the diffusion equation seems to be an insufficient

model for bubbles in the order of several mm. However, in case of small bubbles the performance is much better (cf. Figs. 6(c) and 6(d)), since these bubbles approach the limit of stationary bubble growth much faster.

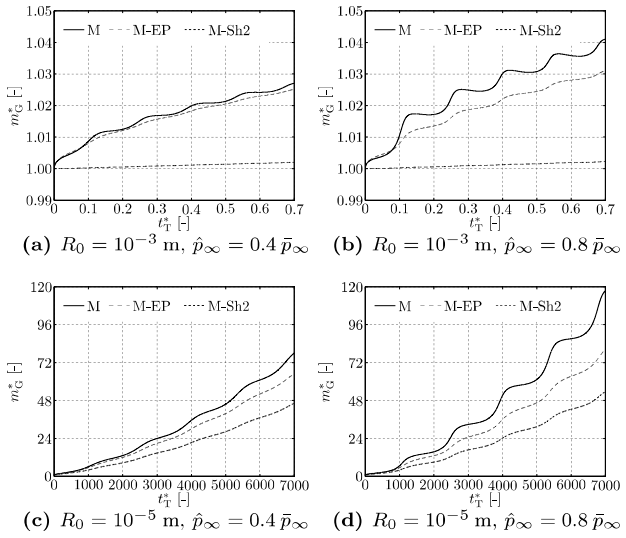

(a) $R_0 = 10^{-3}$ m, $\hat{p}_\infty = 0.4\,\bar{p}_\infty$ **(b)** $R_0 = 10^{-3}$ m, $\hat{p}_\infty = 0.8\,\bar{p}_\infty$

(c) $R_0 = 10^{-5}$ m, $\hat{p}_\infty = 0.4\,\bar{p}_\infty$ **(d)** $R_0 = 10^{-5}$ m, $\hat{p}_\infty = 0.8\,\bar{p}_\infty$

Fig. 6: Bubble growth in an oversaturated solution during moderate pressure oscillations. The ambient pressure is given by $p_\infty = \bar{p}_\infty + \hat{p}_\infty \sin(2\pi f t)$, with $\bar{p}_\infty = 1\,\text{bar}$, $\hat{p}_\infty = 0.4\,\text{bar} \ldots 0.8\,\text{bar}$ and $f = 1\,\text{Hz}$. The Figs. show a comparison of models for different initial bubble sizes and pressure amplitudes, but same dimensionfull period of time and initial degree of saturation $s_0 = 5$.

Fig. 7 shows a comparison of model M and M-EP for finite systems at constant ambient pressure. As discussed before, model M-EP underestimates bubble growth in comparison with model M. This effect is further increased when simulating finite systems. We extend the analytical concentration gradient from Epstein and Plesset in such a way that the concentration difference between the bubble surface and the outer boundary of the system is reduced according to the total mass balance of dissolved air. Clearly, this may not reflect the local concentration profile in the diffusion boundary layer to the full extent but allows us to describe finite systems in a numerically efficient way.

Requirements for air release models may increase for other technical fluids, such as oils that are able to dissolve a higher amount of air in comparison with water, cf. Fig. 7(b). At the same pressure conditions the bubble grows to a greater extent and, thus, induces a more intense velocity field enhancing the effects of advective transport.

5. Conclusion

Simulations of air release have been performed for finite and infinite systems. Different models that vary in the quality of physical modelling and are based on the conservation laws of mass, momentum and energy have been

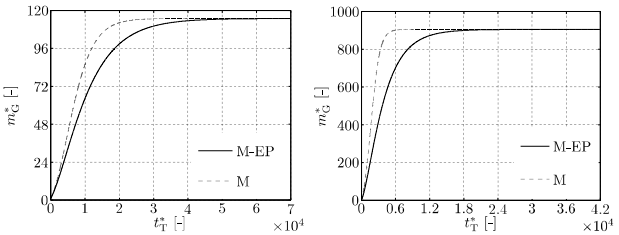

(a) Air-Water **(b)** Air-V1404

Fig. 7: Bubble growth in finite systems ($\frac{R_{\infty,0}}{R_0} = 12.5$, $s_0 = 5$) and for different solute-solvent pairs at constant pressure conditions, $p_\infty = 1$ bar. Fig. 7(b) shows the result of a simulation performed with fluid data of the test oil V1404 produced by Royal Dutch Shell plc.

applied. In particular, we focused on the transport process of dissolved air in the liquid phase. The results have shown the following:

- Slow growth of bubbles with an initial size in the order of several µm can be described by the stationary solution of the diffusion equation in technical applications. Bubbles with an initial size of several mm require a model regarding the history of bubble growth. In turn, one may conclude that the size distribution of bubbles in liquids is of major importance for air release.

- Advection has to be considered for strong pressure gradients, which induce a velocity field around the air bubbles. The diffusion boundary layer is deformed leading to an increased net mass flow of air into the gas phase. This may also lead to complex concentration profiles near the bubble surface.

- The mechanical non-equilibrium has to be considered for pressure excitations near the bubble eigenfrequency f_D. The bubble dynamics may be neglected in the context of air release for excitation frequencies $f \leq 0.1\, f_\text{D}$.

- Thermal effects can be neglected for oscillations outside the eigenfrequency of air bubbles. The enthalpy of solution as well as other energy related fluid properties do not play an important role for common liquids such as water or oils.

Air release models presented in this paper are predictive, i.e. they are solely based on properties that can be determined a priori. This requires the initial size distribution and fluid properties to be known. As a consequence, the formulation of air release depends on an accurate nucleation model. Introducing empirical parameters that are fitted to experimental data might be a way to improve air release models at the expense of the predictive character. Therefore, future work may focus on experimental investigations of air release in technical applications.

Nomenclature

A	Area
a_L	Speed of sound in the liquid phase
c	Molare concentration of the gas
c_p	Isobaric, specific heat capacity
f	Frequency
f_D	Eigenfrequency
H	Henry coefficient of solute-solvent pair
h	Specific enthalpy
Δh_L	Specific enthalpy of solution of solute-solvent pair
M	Molare mass
m	Mass
Nu	Nusselt-Number
p	Pressure
Q	Heat
R	Bubble Radius
$\tilde{R}$	Universal gas constant
r	Spherical coordinate (radius)
$\tilde{r}$	Lagrangian coordinate (radius)
Sh	Sherwood-Number
s	Degree of saturation
T	Temperature
t	Time coordinate
$\tilde{t}$	Lagrangian coordinate (time)
U	Internal Energy
u	Velocity
V	Volume
W	Work due to volume change
z_i	Fluid property

Special characters

β_D	Diffusion coefficient of the gas in the liquid phase
β_T	Thermal diffusivity of the liquid phase
δ_D	Boundary layer thickness
Γ	Boundary of a volume
κ	Heat capacity ratio
λ_L	Thermal conductivity of the liquid phase
ν_L	Kinematic viscosity of the liquid phase
ϕ, θ	Spherical coordinates (angels)
ρ_L	Density of the liquid phase
σ_L	Surface tension of the liquid phase
σ_{rr}	Radial stress
τ_D, τ_T, τ_I	Characteristic time scale of diffusion, thermal diffusion and momentum transfer, respectively

Supscripts

$*$	Dimensionless quantity
0	Reference or initial state
D, I, T	Time scale used to normalise simulation time
G	Gas, bubble surface
∞	Outer boundary
L	Liquid, solvent

References

[1] A. Arefmanesh, S. G. Advani, and E. E. Michaelides. An accurate numerical solution for mass diffusion-induced bubble growth in viscous liquids containing limited dissolved gas. *International Journal of Heat and Mass Transfer*, 35(7):1711–1722, 1992.

[2] H. D. Baehr and K. Stephan. *Heat and Mass Transfer*. Springer, 2006.

[3] E. J. Barlow and W. E. Langlois. Diffusion of gas from a liquid into an expanding bubble. *IBM Journal of Research and Development*, 6(3):329–337, 1962.

[4] C. E. Brennen. *Cavitation and Bubble Dynamics*. Oxford University Press, New York, 1995.

[5] R. Börnstein, H. H. Landolt, K.-H. Hellwege, and O. Madelung. *Heats of Mixing and Solution*, volume 2 of *Landolt-Börnstein. Numerical Data and Functional Relationships in Science and Technology: New series, Group IV Physical Chemistry*. Springer, 1976.

[6] H. S. Carslaw. *Introduction to the Mathematical Theory of the Conduction of Heat in Solids*. Dover Publications, New York, 1945.

[7] A. Eller and H. G. Flynn. Rectified diffusion during nonlinear pulsations of cavitation bubbles. *The Journal of the Acoustical Society of America*, 37(3):493–503, 1965.

[8] P. S. Epstein and M. S. Plesset. On the stability of gas bubbles in liquid-gas solutions. *The Journal of Chemical Physics*, 18 (11):1505–1509, 1950.

[9] W. Heller. *Hydrodynamische Effekte unter besonderer Berücksichtigung der Wasserqualität und ihre Messverfahren*. Institut für Strömungsmechanik, Technische Universität Dresden, 2005.

[10] U. Iben. *Entwicklung und Untersuchung von Kavitationsmodellen im Zusammenhang mit transienten Leitungsströmungen*. VDI Verlag, 2004.

[11] P. J. Linstrom and W. G. Mallard, editors. *NIST Chemistry WebBook, NIST Standard Reference Database Number 69*. National Institute of Standards and Technology, Gaithersburg, Maryland 20899-8420, USA. URL `http://webbook.nist.gov`.

[12] K. Lucas. *Thermodynamik*. Springer, 2004.

[13] A. R. Naji Meidani and M. Hasan. Mathematical and physical modelling of bubble growth due to ultrasound. *Applied Mathematical Modelling*, 28(4):333–351, 2004.

[14] M. S. Plesset and A. Prosperetti. Bubble dynamics and cavitation. *Annual Reviews of Fluid Mechanics*, 9:145–185, 1977.

[15] M. S. Plesset and S. A. Zwick. A nonsteady heat diffusion problem with spherical symmetry. *Journal of Applied Physics*, 23(1):95–98, 1952.

[16] M. S. Plesset and S. A. Zwick. The growth of vapor bubbles in superheated liquids. *Journal of Applied Physics*, 25(4):493–500, 1954.

[17] L. F. Shampine and M. W. Reichelt. The MATLAB ODE suite. *SIAM Journal on Scientific Computing*, 18(1):1–22, 1997.

[18] R. D. Skeel and M. Berzins. A method for the spatial discretization of parabolic equations in one space variable. *SIAM Journal on Scientific and Statistical Computing*, 11(1):1–32, 1990.

[19] Verein Deutscher Ingenieure VDI-Gesellschaft Verfahrenstechnik und Chemieingenieurwesen (GVC). *VDI-Wärmeatlas: Berechnungsblätter für den Wärmeübergang*. Springer, 8. edition, 1997.

[20] E. Wilhelm, R. Battino, and R.J. Wilcock. Low-pressure solubility of gases in liquid water. *Chemical Reviews*, 77:219–262, 1977.

[21] S. Winzer. *Regularisierende Einbettung und Newton-Techniken für Stefan Probleme*. PhD thesis, Institut für Numerische Mathematik, Technische Universität Dresden, 1994.